Springer Oceanography

Najeeb M. A. Rasul
Ian C. F. Stewart *Editors*

Oceanographic and Biological Aspects of the Red Sea

هيئة المساحة الجيولوجية السعودية
SAUDI GEOLOGICAL SURVEY
www.sgs.org.sa

Springer

The Springer Oceanography series seeks to publish a broad portfolio of scientific books, aiming at researchers, students, and everyone interested in marine sciences. The series includes peer-reviewed monographs, edited volumes, textbooks, and conference proceedings. It covers the entire area of oceanography including, but not limited to, Coastal Sciences, Biological/Chemical/Geological/Physical Oceanography, Paleoceanography, and related subjects.

More information about this series at http://www.springer.com/series/10175

Najeeb M. A. Rasul • Ian C. F. Stewart
Editors

Oceanographic and Biological Aspects of the Red Sea

هيئة المساحة الجيولوجية السعودية
SAUDI GEOLOGICAL SURVEY
www.sgs.org.sa

Springer

Editors
Najeeb M. A. Rasul
Center for Marine Geology
Saudi Geological Survey
Jeddah, Saudi Arabia

Ian C. F. Stewart
Stewart Geophysical Consultants Pty. Ltd.
College Park, Adelaide, SA, Australia

ISSN 2365-7677 ISSN 2365-7685 (electronic)
Springer Oceanography
ISBN 978-3-319-99416-1 ISBN 978-3-319-99417-8 (eBook)
https://doi.org/10.1007/978-3-319-99417-8

Library of Congress Control Number: 2018952595

This Springer imprint is published by the registered company Springer Nature Switzerland AG
The registered company address is: Gewerbestrasse 11, 6330 Cham, Switzerland

Preface

The Red Sea has a unique tectonic history, environment and biology. It is a young ocean basin that along its length has undergone or is undergoing the transition from a continental rift to true oceanic seafloor spreading, the nature of which is still open to vigorous debate. In addition, due to its semi-enclosed nature and location within an arid region, the environment is affected by high evaporation rates that, together with limited contact with the Indian Ocean, result in high temperatures and salinities. Lower sea levels in the past have also led to extensive evaporite deposition within its basin. All of this has had a far-reaching impact on the oceanography, marine and terrestrial life of the region.

This is one of a pair of volumes that together follow "The Red Sea: The Formation, Morphology, Oceanography and Environment of a Young Ocean Basin" published in 2015 under our joint editorship. The amount of new information that has become available since then is testament to the range and vigour of research now being carried out in the region, much of it in Saudi Arabia under the sponsorship of the Saudi Geological Survey, and to the level of international interest. Indeed, so much new research has taken place that we have divided the material into two volumes, this one, which concentrates on aspects of the oceanography and biology of the Red Sea, and a second volume concerned with geological, palaeoenvironmental and archaeological issues. A wide range of topics is examined in this volume, and the chapters aim to present some of the current thinking and summaries of research in each field of study, including useful reference lists for further study.

As with the earlier volume referred to above, which was the outcome of a workshop held in Jeddah, Saudi Arabia, in 2013, most of the chapters in this volume were originally presented at a workshop held in Jeddah, from February 15 to February 17, 2016, under the auspices of the Saudi Geological Survey (SGS), and have been independently reviewed, revised and edited for publication.

Dr. Peter Vine's wide-ranging contributions to this volume deserve special mention. We are indebted to him for his knowledge of key topics of Red Sea ecology and in particular for assistance in preparing chapters on the Red Sea's endemic fish and dugongs. We are pleased to include a personal perspective on some of his own studies which we hope will stimulate further research in the fields he discusses.

We would also like to mention Dr. John E. Randall who is a Senior Ichthyologist Emeritus at the Bishop Museum, Honolulu, and is a co-author of the chapter on endemic fishes of the Red Sea. He has been carrying out research in marine zoology since obtaining a B.A. in 1950 from UCLA and a Ph.D. in marine zoology in 1955 from the University of Hawai'i. He has received numerous awards for his work, served on the editorial board of several journals and remains as editor of the scientific series he founded, Indo-Pacific Fishes. He has over 900 publications, including 13 guidebooks on fishes. He has described 799 valid new species of marine fishes.

The support of the Survey in the preparation of this volume is greatly appreciated, and we would like to thank all those who have been involved in its production. We would especially like to thank Dr. Zohair A. Nawab, former President of SGS, and Dr. Abdullah M. Alattas, former Assistant Vice President, as well as Eng. Hussain M. Al Otaibi, President of SGS and

Mr. Salah A. AlSefry, Assistant Vice President for Technical Affairs. Colleagues at the SGS and the Center for Marine Geology are also thanked for making the workshop a success. Mr. Louiesito Abalos played a substantial part in the preparation of material for publication. Finally, we acknowledge the contributions of the technical referees to improving the contents of the chapters together with the assistance of Viju Falgon Jayabalan and Banu Dhayalan (Project Coordinator), Janet Sterritt-Brunner (Production Books Project Coordinator) and Dr. Nabil Khélifi, (Senior Editor, of Springer Nature) in preparing this volume for publication.

Jeddah, Saudi Arabia — Najeeb M. A. Rasul
Adelaide, Australia — Ian C. F. Stewart

Contents

Introduction to Oceanographic and Biological Aspects of the Red Sea

1

Najeeb M. A. Rasul, Ian C. F. Stewart, Peter Vine and Zohair A. Nawab

Location, Bathymetry and Statistics

This volume builds on the success of a previous publication, "The Red Sea: The Formation, Morphology, Oceanography and Environment of a Young Ocean Basin", edited by Rasul and Stewart (2015), in which an extensive introduction (Rasul et al. 2015) outlined the main features of the Red Sea, including aspects of the oceanography and biology which will not be repeated here in detail.

The Red Sea is a semi-enclosed, elongated body of relatively warm water, about 2000 km long with a maximum width of 355 km, a surface area of roughly 458,620 km^2, and a volume of ~250,000 km^3 (Head 1987). The Red Sea is bounded by nine countries, with numerous coastal lagoons, a large number of islands of various dimensions and extensive groups of shoals; it is bifurcated by the Sinai Peninsula into the Gulf of Aqaba and the Gulf of Suez at its northern end (Fig. 1.1). The sea is connected to the Arabian Sea and Indian Ocean via the Gulf of Aden in the south through the narrow Strait of Bab el Mandab, which has a minimum width of only 30 km, where the main channel is about 310 m deep and 25 km wide at Perim Island (Morcos 1970). Although the Hanish Sill at 13°44′N has a maximum depth of only 137 m, it is likely that the Red Sea has remained connected to the Gulf of Aden for at least the past 400,000 years (Lambeck et al. 2011). However, during the Last Glacial Maximum (LGM), the water depth over the Hanish Sill is estimated to have fallen to only 25–33 m (Biton et al. 2008; Lambeck et al. 2011), with considerable effects on the Red Sea circulation and ecology (Trommer et al. 2011).

The Red Sea has three distinct depth zones; shallow shelves less than 50 m in depth (about 25%), deep shelves with depths ranging between 500 and 1000 m, and the central axis with depths between 1000 and about 2900 m. The continental slope has an irregular profile, with a series of steps down to about 500 m depth. The 15% of the Red Sea that forms the narrow axial trough is over 1000 m in depth and contains a number of bathymetric depressions or Deeps, some containing hot saline brines (e.g., Hovland et al. 2015) and metalliferous sediments that were formed by the spreading of the sea. Recent data along the axis (Augustin et al. 2014) suggest that the western Suakin Deep, with a depth of 2860 m at 19.6° N is the deepest part of the Red Sea Rift. The seismically active Gulf of Aqaba is 160–180 km long and 19–25 km wide, narrow in the north and widening to the south with maximum depths of 1850 m toward the east, where shelves and coastal plains are absent. The Gulf of Suez is a 300 km long, 25–60 km wide, shallow flat bedded basin with depths ranging between 50 and 75 m. Depths increase toward the south but remain under the 100 m mark at the confluence of the Red Sea and do not exceed 200 m.

The Red Sea is one of the youngest oceanic zones on earth, and along most of its length it forms a rift through the Precambrian Arabian-Nubian shield. The southern end of the Red Sea joins the Gulf of Aden spreading centre and the northern end of the East African Rift Zone at a triple junction in the Afar region, an area with extensive volcanism. In the early stages of rifting, prior to a permanent connection to the Gulf of Aden, thick evaporite deposits accumulated in the Red Sea, and on the shelf and marginal areas these deposits are overlain by recent sediments. The sea only turned into an open marine environment when the Gulf of Suez in the north and Indian Ocean in the south became connected in the Pliocene.

N. M. A. Rasul (✉)
Center for Marine Geology, Saudi Geological Survey, Jeddah, Saudi Arabia
e-mail: najeeb_rasul@hotmail.com; ; rasul.nm@sgs.org.sa

I. C. F. Stewart
Stewart Geophysical Consultants Pty. Ltd., Adelaide, SA, Australia

P. Vine
Earth and Ocean Sciences, School of Natural Sciences, NUI Galway, Galway, Ireland

Z. A. Nawab
Saudi Geological Survey, Jeddah, Saudi Arabia

N. M. A. Rasul and I. C. F. Stewart (eds.), *Oceanographic and Biological Aspects of the Red Sea*,
Springer Oceanography, https://doi.org/10.1007/978-3-319-99417-8_1

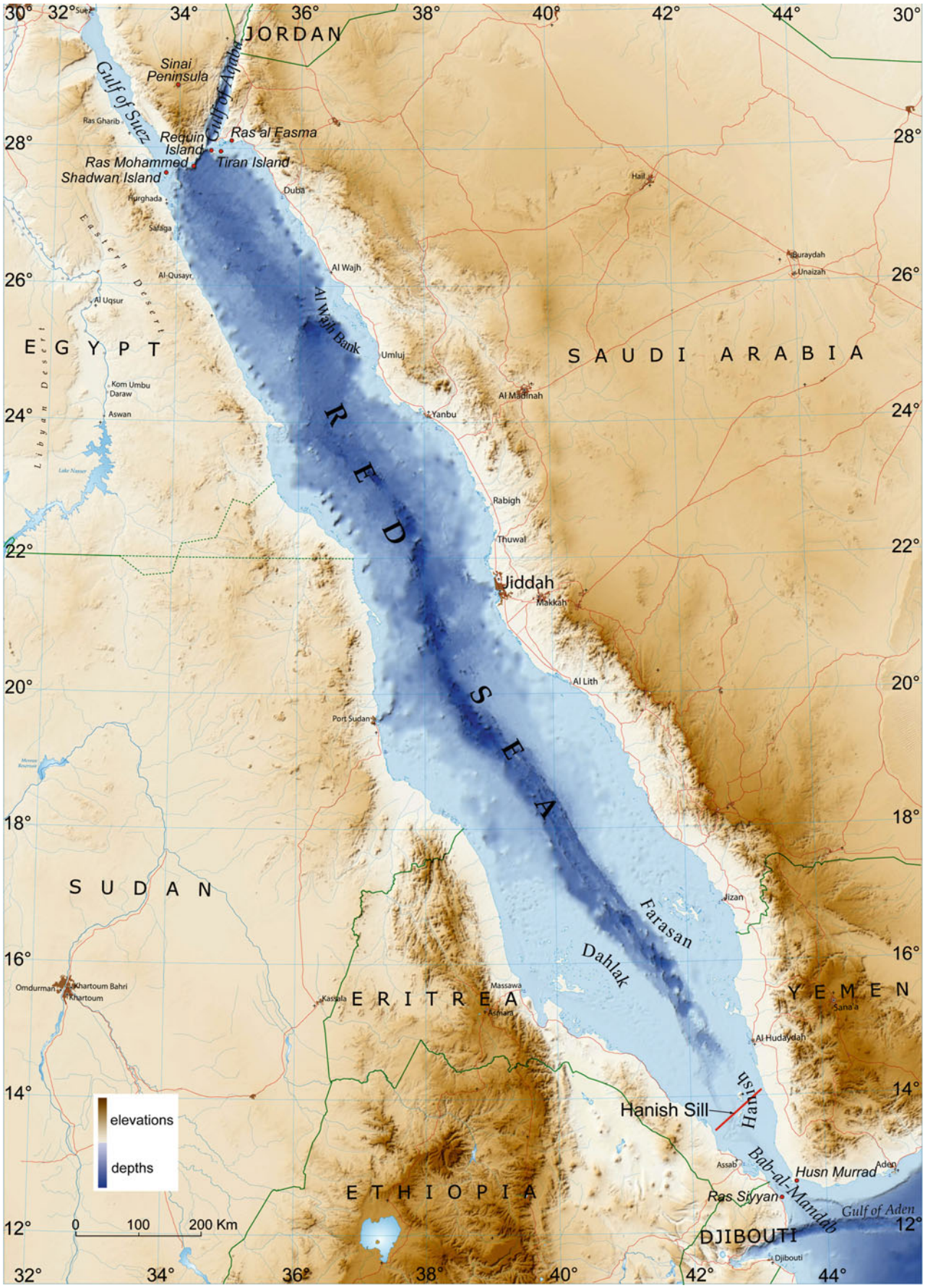

Fig. 1.1 Geographic map of the Red Sea area, where darker colours indicate greater depths or higher elevations (after Rasul and Stewart 2015)

Chapters in this Volume

This volume is arranged into two main sections, the first dealing with the Red Sea's oceanography and the second covering biological research. It has been built around a workshop (held in 2016) hosted by the Saudi Geological Survey and includes contributions from experts working in Saudi Arabia, Egypt, Sudan, India, the United Kingdom, Ireland, France, Russia, the United States, New Zealand, Hong Kong, Italy, and the Falkland Islands. Despite this eclectic mix of Red Sea related topics, reflecting divergent lines of active research, there are several overlapping themes, in particular the fact that there are more questions than answers in our present knowledge of Red Sea marine biology.

Oceanography

Eleven chapters deal with various aspects of the Red Sea's oceanography, including tidal movements, properties of sea water, organic tracers in sediments, nitrogen, phosphorus and carbon in coastal waters, satellite studies on coral reef induced turbulence, the dynamics of coastal lagoons, hydrocarbons in Obhur lagoon sediments, metal contaminants in Saudi Arabia's coastal waters, calcite and aragonite saturation levels in Yemen's coastal waters, the geochemistry of brine-filled deeps, and desalination in Yemen.

The Red Sea's tidal movements are relatively small with semi-diurnal spring tides reaching a vertical range of about metre at the northern and southern extremities and "a central amphidrome, zero tidal range, between Jeddah and Port Sudan". David Pugh and his colleagues have created a new tidal model for the Red Sea. This is the first publication of their data and the model they produced is: (i) depth integrated and two dimensional, (ii) driven by Indian Ocean tidal boundary levels and eight tidal constituents, (iii) has a much higher resolution than any previous models, (iv) was run for a year to give high resolution of tidal frequencies, and (v) has a depth-independent friction drag coefficient of 0.003. They used the model to compare with actual readings inside and outside the Red Sea, and conclude that "future modelling, necessarily three-dimensional, may address and incorporate the impact of direct gravitational forcing, and reduce small but systematic differences for observations. Meanwhile, the results published here represent a major advance on any previously published tidal representations".

Red Sea waters are well known for their clarity, especially in the northern Gulf of Aqaba. Manasrah and his co-workers examine the physical and chemical properties of seawater in the Gulf and Red Sea and provide a comprehensive presentation on the forces at work in shaping these waters, from meteorology to physical and chemical oceanography. The importance of a thermocline in maintaining the oligotrophic nature of surface waters is mentioned repeatedly and often in the context of there being a a seasonal cycle of stratification in spring, maintenance of a shallow thermocline in summer, and subsequent deepening of the thermocline to produce "deep mixed layers in winter". Some of the facts presented demonstrate key characteristics of the Gulf of Aqaba where evaporation amounts to between 0.5 and 1.0 cm per day; the pH is fairly constant at around 8.3 due to the buffering effects of calcium carbonate deposited by corals, and higher salinity levels result in density gradients. Higher concentrations of nutrients, chlorophyll *a,* ammonium, nitrates, nitrite, phosphates, and silicates in the Gulf of Aqaba in winter—due to mixing of the water column—all contribute toward enhanced primary productivity, resulting in higher phytoplankton abundance and increased chlorophyll *a* concentrations. Meanwhile, the authors comment that oxygen levels in the Gulf show a regular pattern, inversely proportional to that of temperature, exhibiting a well-balanced profile in terms of respiration and photosynthesis and a high level of ventilation (mostly 100%) "due to annual deep mixing".

Rushdi and colleagues present a study and analysis on the sources of externally derived organic matter in the Red Sea. In order to do so they sampled dust, surface sea water particulate matter and coastal sediments, examining the extractable organic matter (EOM). Their findings are based on key parameters and molecular marker analysis enabling them to deduce the likely source of the various inputs, many of which are from natural sources such as plant debris. Dust is a major carrier with six million tons deposited into the Red Sea each year. In fact, the regional dust belt associated with low-latitude African and Asian deserts is the largest source of dust on our planet. Dust storms, that can be common in summer along both coastlines, carry vast quantities of nutrients, impacting oligotrophic waters such as those of the northern Red Sea. Whilst storms are natural events, they may carry pollutants resulting from human activities. An assortment of chemical compounds associated with dust and surface sediments were used to identify the likely source of associated pollutants. The compounds are mainly *n*-alkanes from both natural and anthropogenic sources, *n*-alkanoic acids, *n*-alkanols, methyl n-alkanoates, steroids, hopanes, steranes and UCM (unresolved complex mixture of branched and cyclic hydrocarbons) from petroleum inputs, and plasticizers which are all from anthropogenic sources. The presence of *n*-alkanes indicated un-degraded crude oil, whilst petroleum products in general are indicated by the biomarkers hopane and sterane hydrocarbons. Plasticizers can be released to the environment due to bio- and photo-degradation and are present in the dust. Overall, the authors concluded that both natural and anthropogenic components contribute to organic

inputs in the Red Sea. The latter are most important in sediments where, depending on the location and types of human activity, they can exceed 30%.

The Red Sea is generally nutrient deficient (oligotrophic) and depends on inflow from the Indian Ocean, via Bab al Mandab, for most of its nitrogen and phosphorus. Concentrations of these decline northward, with peaks near coastal cities such as Jeddah where the impact of effluent outflows and industrial activities can be observed. Al-Farawati and his colleagues present their findings regarding the distribution, sources, and biogeochemical processes that control levels of dissolved inorganic phosphorus, dissolved inorganic nitrogen (nitrates, nitrites, ammonium) and dissolved organic carbon (DOC). They also calculated the contribution to the total nitrogen-phosphorus budget from anthropogenic sources. There is a distinct seasonality in dissolved and particulate carbon levels (DOC and POC), connected to peaks in primary production, with higher values in late spring. Nitrogen levels were dominated by ammonium in autumn (60% of total inorganic nitrogen, TIN) and nitrates in spring (62% of TIN). Anthropogenic nitrogen and phosphorus, mostly associated with sewage discharges into Jeddah's coastal waters, account for 0.9% and 9.9% respectively of the deficit of the two elements through the Red Sea/Indian Ocean exchange process at the Strait of Bab al Mandab. These elements are directly linked to the capacity of the water-body to support phytoplankton which deplete dissolved levels of nitrogen and phosphorus—potentially limiting factors for primary production. Exhaustion of nitrogen or phosphorus stops development of phytoplankton whilst exhaustion of silicate stops development of diatoms. The authors point out the importance of correctly identifying the limiting nutrient in coastal waters since it can determine the type of sewage treatment most appropriate for each situation. In turn, this will help to minimise costs and reduce ecological impact of sewage effluent on coastal marine life. They do however point to various difficulties with determining which nutrients are limiting factors and urge caution in reaching conclusions in this regard.

The use of optical remote sensing systems to map and monitor surface and shallow water topography is well established but has been limited by a number of factors, ranging from availability and access to suitable satellites, to regularity and resolution of the images produced, effects of weather (especially cloud cover), water clarity (impacted by plankton and turbulence), limitations of depth penetration, and the need for proven algorithms that deliver reliable detection of selected criteria. Marghany and Hakami tested the suitability of the relatively new Flock-1 satellite system, launched in 2014 (comprising 28 tiny satellites), to detect the locations and main characteristics of some Red Sea coral reefs. This was the first time that Flock-1 had been used for oceanographic surveys. They subjected the data to a 'multi objective evolutionary algorithm' (MOEA) developed to automatically detect the patterns of water disturbance ('turbulent boundary flow') overlying coral reefs—mainly on the Al-Wajh bank and Farasan Islands, off Saudi Arabia. Their results underline the 'added value' that can be gained from Flock-1 with potential implications for maritime activities including shipping and fishing together with sediment and pollution tracking. The authors examined two hypotheses; firstly, that low radiometric resolution data such as that produced by Flock-1 can be used for surface and benthic coral features detection, and secondly that such machine learning and intelligent algorithms are able to accurately detect dynamic interactions between sea surface movement and benthic features such as coral reefs. The Flock-1 satellites, each measuring $30 \times 10 \times 10$ cm, are equipped with cameras capable of taking pictures with a ground resolution of 3–5 m and visible spectra of 400–660 nm and near infrared 700–900 nm. In order to ground truth their results, the team used maps of Saudi Arabian coral reefs published in the Khaled bin Sultan Living Oceans Foundation Atlas of Saudi Arabian Red Sea Marine Habitats. When it comes to automatically detecting the water movements created by the hugely varied forms of coral reefs there is no 'one size fits all solution'. Instead the authors developed an MOEA that preserved the diversity of the solution set. Overall, the authors present a compelling case for greater use of Flock-1 data in Red Sea reef studies, using an MOEA.

Moving from offshore reefs and shoals to coastal indentations in the form of lagoons, the characteristics of coastal lagoons, both in general and with particular reference to the Saudi Arabian Red Sea, are described by Albarakati and Ahmad. They studied water column conditions of Rabigh lagoon and the flushing times of Shoaiba, Obhur, Ras Hatiba, Rabigh and Yanbu. In Rabigh they found that the water column remains mixed (rather than stratified) throughout most of the year, with the possible exception of September to October when a weak stratification may appear. Flushing times of the various lagoons ranged from a few days to a month. Coastal lagoons can be among the most productive ecosystems in the biosphere. Turning to Saudi Arabia's coastal lagoons, they emphasise the high levels of biological productivity in these increasingly threatened environments and call for more studies and constant monitoring in order to ameliorate the stresses caused by human activities. Coastal lagoons of the Red Sea receive waste from the increasing levels of anthropogenic activity and some are used as intakes for desalination plants. "They contain different types of vegetated habitats, such as sea grasses or mangroves, which should be preserved as natural grounds for productivity." The present levels of stress will rise even higher as a result of climate change and global warming. The authors call for involvement of a "wide variety of institutes and administrative units as well as research in a range of scientific

disciplines in association with those involved with the lagoons."

Ahmed Rushdi and his colleagues analysed surface sediment samples from Obhur Lagoon on the Red Sea coast of Saudi Arabia to determine the levels, distribution and sources of hydrocarbon compounds, the main sources of which were anthropogenic petroleum products and plasticizers, with lesser amounts from biogenic sources, including natural waxes of terrestrial higher plants and marine microbial detritus. The anthropogenic inputs of the total lipid hydrocarbons for all sediments ranged from 14 to 98% for petroleum products and from 2 to 18% for plasticizers, and biogenic inputs ranged from 0 to 10.7% for terrestrial higher plant waxes and from 0 to 68.5% for marine microbial detritus. The petroleum residues and plasticizers in the sediments probably affect the marine ecosystems and associated species groups that use the lagoon as a coastal nursery and spawning area.

Further offshore, Karuppasamy et al. analysed surficial sediment samples from sixty stations between 23°N and 28°N latitudes in the northern Red Sea for 10 metals. Arsenic was the only element to exhibit exceedance with 88% of the stations above upper continental crust concentrations. A sediment contamination assessment was carried out using the geoaccumulation index (Igeo) and enrichment factor (EF), and the ecological hazard was assessed using the Adverse Effect Index (AEI), Potential ecological risk factor (ER) and Potential ecological index (RI). Using statistical analyses, the stations were grouped as "uncontaminated", "minor enrichment", "metallogenic enrichment" and "anthropogenic enrichment".

Seawater samples from different depths at eight stations along the Red Sea coast of Yemen were collected by Rushdi et al. during early winter for the determinations of the temperature, salinity, pH value and total alkalinity profiles. The results showed that the surface seawater layers were several-fold supersaturated with respect to both calcite and aragonite and suggest that low magnesian calcite and aragonite are likely the major carbonate solid phases formed under current saturation levels. Recent studies show that the present oceanic pH values may drop by 0.1 and 0.4 units in 50 and 200 years, respectively. This will affect the morphology and mineralogy of calcium carbon deposits as well as the distribution of calcifying organisms in the region. Further studies are warranted to investigate the occurrence, distribution and mineralogy of corals and the effects of physical and chemical parameters upon their growth in the region.

Antunes et al. investigate the geochemistry and life at the interfaces of the brine-filled deeps in the Red Sea where the extreme environments form characteristically steep gradients across the brine-seawater interfaces. Due to their unusual nature and unique combination of physical-chemical conditions these interfaces provide an interesting source of new findings in the fields of geochemistry, geology, microbiology, biotechnology, virology, and general biology.

Turning to onshore water matters, Minissale et al. examine the consumption and uses of water in Yemen, which has a declining water table with the Mesozoic-Cenozoic aquifer unable to support irrigation and the geothermal reservoir too will decline due to excessive withdrawal of water. A solution to this problem is to develop the geothermal resources around Damt and Dhamar to support desalination of the Red Sea and Gulf of Aden seawater to generate electricity and fresh water to contribute to the country's food and energy security and reduce dependence on food imports.

Biology

The biology section of this volume is a valuable contribution to our knowledge and understanding of this fascinating marine biosphere, with sixteen chapters throwing light on such divergent, yet interconnected, topics as Crown of Thorns starfish, algal-coral and sponge-coral interfaces, the ecological impact of aggressive damsel fish, endemic fishes, sharks, cetaceans, dugongs, macrobenthos, seagrasses, coral diseases, microbial activity, mangroves, pearl oysters, copepods, zooplankton, phytoplankton, turtles and, most appropriately, the growing role of 'citizen science'.

Studies of Crown of Thorns starfish, aggressive damselfish, pink coralline algae and the 'turf wars' that take place between corals, sponges and algae are all covered in a reflective chapter by Peter Vine that looks back at some early research in these fields and shows how our understanding of the dynamics of reef ecology has advanced. Perhaps of greatest importance in this chapter is the author's highlighting of the important role played by crustose coralline algae, CCA, not just in binding the reef structure, but also in providing suitable settlement surfaces on reefs where voracious cnidarians pose a threat to most larval forms in search, excuse the anthropogenic assumption, of a 'safe home'.

The present number of fishes recorded from the Red Sea is 1166 species from 159 families whose habitats range from shallow to deep waters; among these 165 species are exclusively endemic to the Red Sea. The authors of the chapter on endemic Red Sea fishes are themselves record breakers: Dr. J.E. Randall, still contributing to scientific literature at the age of 94, and Sergey Bogorodsky, a much younger man with a passion for his subject that is complimented by an attention to taxonomic detail and a high level of photographic expertise. Randall's statistics are noteworthy with 902 published papers, 48 of which are on Red Sea fishes. He has described and named 799 new species of fish and has written 13 regional fish guides, including "Red Sea

Reef Fishes" that is a must-have book for Red Sea divers and marine scientists. Most of his work is accompanied by sharply focused and expertly lit photographs of fresh specimens with the fins carefully pinned out to enable identification. Several species of fish that are commonly found in the Red Sea are shown in Figs. 1.2, 1.3, 1.4 and 1.5.

Julia Spaet calls for urgent regional efforts to assess the status of Red Sea sharks, and the development and implementation of "effective management plans to ensure socio-ecological sustainability". The author notes the presence of 29 shark species in the Red Sea and summarises what is known of these species. She makes a strong case for further studies and conservation efforts before some of the most threatened species disappear from these waters.

It is a similar story with cetaceans, of which at least 16 species are found in the Red Sea, and Marina Costa and colleagues point out that we still do not have a clear picture

Fig. 1.2 The blue masked butterflyfish, *Chaetodon semilarvatus*, ranges from the Red Sea (type locality, Massawa) and Gulf of Aden to southern Oman. It inhabits reefs of rich coral growth from depths of about 1–20 m and is often seen in pairs, occasionally in small aggregations. It tends to be inactive most of the day, hovering beneath ledges or plates of *Acropora* corals, feeding on polyps of hard and soft corals late in the afternoon (pers.comm. JE Randall and S Bogorodsky). Photo © Hans Sjoeholm

Fig. 1.3 Juvenile of the Yellowbar Angelfish, *Pomacanthus maculosus*, occurs in the Red Sea (type locality, Luhaiya, Yemen), east to the Gulf of Oman and Arabian Gulf, south to Mozambique and the Seychelles, and has even been reported from the Mediterranean Sea by Bariche (2010). It usually occurs on sheltered, often silty, coral reefs, at depths of 4–20 m. It is solitary and adults are easily approached. Feeds on sponges and algae. Photo © Hans Sjoeholm

of the Red Sea's whales and dolphins, particularly in the central and southern areas. They say that there is an "urgent need for a more up-to-date appraisal of cetaceans, including the presence, abundance, distribution and behaviour of represented species throughout the Red Sea" and state that there is a "duty of care for governments, NGOs and academic institutions within the region to support and facilitate the research required to acquire a better understanding of the Red Sea's whales and dolphins."

Meanwhile, Maddalena Fumagalli and colleagues throw more light on one of the erstwhile 'unknowns' of Red Sea dolphins: where and when do they sleep? They point out that disturbance by humans, in for example tourist dolphin watch boats, can lead to sleep deprivation, impacting individual physiology and cognitive abilities. This can have "long term detrimental consequences on wild dolphin populations". In the Red Sea the authors state that scientific studies on the impacts on dolphins are still preliminary, but the Samadi

Fig. 1.4 Harlequin filefish *Oxymonacanthus halli* and Rueppell's wrasse *Thalassoma rueppellii* over an outcrop of coral. The harlequin filefish is endemic to the Red Sea; type locality, Sanafir Island, Gulf of Aqaba. It occurs on reefs with luxuriant coral growth in lagoons, bays and sheltered seaward reefs from depths of 0.5–30 m; usually seen in pairs among branches of *Acropora* corals; feeds on coral polyps; also takes refuge in fire coral (*Millepora*). Closely related to *Oxymonacanthus longirostris* (Bloch & Schneider), wide-ranging in the rest of the Indo-Pacific region. Rueppell's wrasse is also endemic to the Red Sea; type locality, El Quseir. It occurs on coral reefs and adjacent habitats from 0.5 to 20 m and is reported to feed mainly on benthic invertebrates, occasionally on small fishes. It is unafraid of divers, apparently attracted to the disturbances they often make to the substratum (pers.comm. JE Randall and S Bogorodsky). Photo © Hans Sjoeholm

Fig. 1.5 The Crown Butterflyfish (*Chaetodon paucifasciatus*) is known only from the Red Sea (type locality, El Quseir, Egypt) and the Gulf of Aden where it is found on coral reefs and adjacent habitats at depths from 1 to 30 m, usually in pairs, sometimes in small groups. Omnivorous, feeding on polyps of hard and soft corals, algae, small crustaceans, and polychaete worms (pers.comm. JE Randall and S Bogorodsky). Photo © Hans Sjoeholm

Reef protection zone in Egypt is setting an example of how to manage this issue. They highlight the importance of identifying and protecting well established dolphin resting areas.

The chapter by Nasr et al. on dugongs highlights the extent to which we are still guessing at important issues such as population status of these herbivorous marine mammals in the Red Sea. It also demonstrates what can be achieved by the concentrated efforts of a few individuals over a relatively short period of time. Hopefully, the recent survey work carried out in Egypt will be extended to other countries bordering the Red Sea. The authors repeat the assertion of previous expert studies that have described our overall knowledge of Red Sea dugongs as 'Data Deficient'—an admission that reflects disappointingly on the administration of research on dugongs in this region over the past few decades. Emphasis on gaps in our knowledge and calls for further studies in their particular fields were made by several other authors.

Thadickal Joydas and co-authors remind us that despite their importance and the unique characteristics of their habitat (high temperature, high salinity, oligotrophic conditions) "benthic studies conducted in the deep-sea environments of the Red Sea are few".

Turning to shallow water habitats Mohammad Qurban and co-workers provide an overview of the presence and distribution of seagrasses in the Red Sea. They too point to the dearth of scientific literature in this field, stating that "there is little information on seagrass diversity and distribution in the Saudi Arabian coast of the Red Sea".

The theme is reiterated by Amin Mohamed and Michael Sweet who review current knowledge of coral diseases in the Red Sea. They write that "despite their reported significance in reefs around the world, the aetiologies of the majority of diseases are still unknown and coral epidemiology remains poorly understood". Initial triggers for coral diseases, frequently involving bacteria, viruses, fungi or protozoa, are abiotic factors such as temperature, UV exposure or pollution, and the impact of coral predation resulting in feeding scars. It seems that "diseases affecting corals throughout the Red Sea are one of the least well explored and documented."

Anna Roik and colleagues present a study that highlights the physical and chemical impact on microbial community patterns which, in turn, affect coral reef growth. Their observations of the surface coverage of bacteria and algae—the "epilithic biofilm"—"crucial for the recruitment of reef-builders" shows how these are influenced by seasonally variable factors such as temperature, salinity, and dissolved oxygen. Bacteria from the genus *Endozoicomonas* are particularly prevalent in central Red Sea corals and are sensitive to anthropogenic disturbances, thus providing an early warning of the impact of humankind on the Red Sea's reefs. Meanwhile, endosymbiotic dinoflagellates in central Red Sea corals, vital for driving the calcification (and reef growth) process, are dominated by *Symbodinium*. They note that reef growth slows during summer months, probably because sea temperatures approach the upper tolerance levels for their symbiotic algae ("as evidenced by repeated mass-bleaching events during recent years"). Such baseline studies provide valuable frameworks for understanding the influences at play in terms of the ebb and flow of coral development and "for quantification of the impacts of environmental change in the region".

In addition to corals and sea-grasses, the Red Sea's sheltered bays and shorelines are natural habitats for mangrove trees that play a vital role in creating organic rich habitats for juvenile fish and crustaceans. Unfortunately, coastal development projects have paid little heed to the environmental contribution that mangroves make to the marine ecosystem. Ahmed Khalil has studied the small benthic invertebrates (meiofauna) that live in association with Sudan's mangroves, including species of copepods, nematodes, ostracods, mud-dragons (Kinorhyncha), worms (Oligochaeta), flatworms (Platyhelminthes), jaw worms (Gnathostomulida), hairybacks (Gastrotricha) and cnidarians. He looked in particular at what happens to this diverse meiofaunal community when mangrove trees are chopped down and partially or completely cleared. Deforested sites had higher densities of copepod/nauplii and decreased nematodes. An increase in abundance of many forms was noted in the partially deforested sites. Removing mangroves caused a "decline in the efficiency of the ecosystem function as a nursery ground for marine organisms, which represents one of the vital services provided by the mangrove ecosystem."

Among the larger species that are sometimes found clinging to the roots of mangroves is the pearl oyster, *Pinctada margaritifera*, which has been the subject of several mariculture projects in Dungonab Bay on Sudan's northern Red Sea coastline. Spat are collected on ropes suspended from rafts in July and August and are then transferred to nursery trays. They are held in these until they are ready for on-growing in larger trays near Dungonab village. Biological research on Sudan's pearl oysters has been carried out over many years by the author of this chapter, Dirar Nasr, who presents the most recent observations on the species, based primarily on his own research. Heavy settlement of oyster spat in Dungonab Bay is a quite unusual feature, not seen elsewhere in the Red Sea and possibly unique in terms of the scale of larval settlement of *P. margaritifera* throughout its range. It contrasts quite sharply with the situation regarding plankton elsewhere in the Red Sea where oligotrophic conditions do not generally favour such impressive planktonic concentrations.

Two chapters in this publication take a timely look at plankton of the Red Sea. Ali Al-Aidaroos and colleagues present their findings on that most important link in the food chain, Copepoda, and Maher Amer presents a more general review of the zooplankton. An important source of the Red Sea's plankton is the Indian Ocean whose waters in areas adjacent to the southern entrance of the Red Sea are recipients, via upwelling, of nutrient rich colder water. Carried into the Red Sea on northward flowing waters, these oceanic zooplankters encounter increasingly hostile conditions in terms of raised salinity and temperatures, compounded by decreased nutrient levels. These distinctive environments tend to promote endemicity in those forms that are adapted to meet the environmental challenges of the central and northern Red Sea.

The important role played by copepods in linking primary producers with secondary consumers can hardly be over-emphasised. They are an extremely diverse group found in almost every available habitat. Over 970 species of planktonic copepods occur in the Indian Ocean with 276 found, according to this recent study by Al-Aidaroos and colleagues, in the Red Sea. Indeed, "the epipelagic zone in the Red Sea is usually dominated by copepods", particularly in the southern half of the Red Sea during winter months when mesozooplankton are at their peak. The authors show how copepods are vulnerable to Ultraviolet-B radiation and may symbiotically influence growth and development of the Red Sea's coral reefs and their associated biota.

Contrasting with most topics covered in this volume, the author of 'Zooplankton of the Red Sea', Maher Amer, is able to direct the reader's attention to a significant number of studies, dating back to the beginning of the 19th century,

including a number of major oceanographic expeditions. He lists 111 references and presents results from his own plankton sampling in the northern Red Sea. It is generally agreed that there is a decline in neritic species from south to north, and also that demersal plankton are most abundant in close proximity to coral reef patches as opposed to open water. The abundance of plankton in shallow depths is also much greater at night time. Furthermore, in accordance with other studies, it was found that copepods were the most abundant group among demersal zooplankton, accounting for 58.7% of the total, highlighting their importance in the food chain.

The few studies on phytoplankton and primary production in the Red Sea mostly cover only limited areas. Qurban et al. review previous studies and show that the levels of biomass and production in the Red Sea are relatively low, with a north-south gradient and a distribution that is influenced by anticyclonic eddies, in which biomass and production are twice as high as those elsewhere, suggesting that the notion that the Red Sea is oligotrophic needs to be revised. The phytoplankton diversity is quite high, and with additional records of 74 species from the samples in four cruises, the current inventory of phytoplankton stands at 463 species. The review also suggests prospective avenues of phytoplankton research in the Red Sea waters.

The manner in which data for science is gathered has changed over the centuries. Increasingly, scientists are tapping into the time, knowledge, expertise, enthusiasm and opportunity that untrained or lightly supervised 'amateurs' can bring to various field studies. In addition to increased use of monitoring tools such as audio-visual recording and aerial drone surveys, the introduction of 'citizen scientists' can create valuable data sets in some of the most remote or difficult habitats. This theme is explored by Agnese Mancini and Islam Elsadek in their presentation on monitoring megafauna in the Red Sea. They point to the previously untapped resource of safari boats and diving operations that visit reef sites on a daily basis and whose operatives are likely to be interested in, and cooperative with, organised surveys. "Engaging with this sector and creating long lasting partnerships for data collection through simple protocols could be a winning approach to obtain important information from remote areas and/or on rare species." They applied this approach (in 'Turtle Watch Egypt') to surveying turtle populations in the northern Red Sea, completing 2448 observation reports at 157 sites and recorded 1038 sightings of turtles belonging to four species: hawksbill, green, loggerhead, and olive ridley. The research provides a valuable model for future surveys of megafauna in other areas where commercial activities, such as dive tourism, bring people out on the sea on a frequent basis.

This volume offers a wide range of fascinating studies on Red Sea marine life. Together with the previous volume, it provides a valuable resource for future scientific investigations. It is also a poignant reminder that humankind is blessed by rich, diverse and intricately connected biotopes. If there is an overarching theme or message in these pages it is to appreciate the prolificacy of nature, to better understand its complexity, and to protect the extraordinary environments and species that form our unique planet.

References

Augustin N, Devey CW, van der Zwan FM, Feldens P, Tominaga M, Bantan RA, Kwasnitschka T (2014) The rifting to spreading transition in the Red Sea. Earth Planet Sci Lett 395:217–230. https://doi.org/10.1016/j.epsl.2014.03.047

Bariche M (2010) First record of the angelfish Pomacanthus maculosus (Teleostei: Pomacanthidae) in the Mediterranean. Aqua 16(1):31–33

Biton E, Gildor H, Peltier WR (2008) Red Sea during the last glacial maximum: implications for sea level reconstruction. Paleooceanography 23, PA1214. https://doi.org/10.1029/2007pa001431

Head SM (1987) Red Sea fisheries. In: Edwards AJ, Head SM (eds) Red Sea: key environments. Pergamon Press, Oxford, pp 363–382

Hovland M, Rueslåtten H, Johnsen HK (2015) Red Sea salt formations—a result of hydrothermal processes. In: Rasul NMA, Stewart ICF (eds) The Red Sea: the formation, morphology, oceanography and environment of a young ocean basin. Springer Earth System Sciences, Berlin Heidelberg, pp 187–203. https://doi.org/10.1007/978-3-662-45201-1_11

Lambeck K, Purcell A, Flemming NC, Vita-Finzi C, Alsharekh AM, Bailey GN (2011) Sea level and shoreline reconstructions for the Red Sea: isostatic and tectonic considerations and implications for hominin migration out of Africa. Quatern Sci Rev 30:3542–3574

Morcos SA (1970) Physical and chemical oceanography of the Red Sea. Oceanogr Mar Biol Annu Rev 8:73–202

Rasul NMA, Stewart ICF (eds) (2015) The Red Sea: the formation, morphology, oceanography and environment of a young ocean basin. Springer Earth System Sciences, Berlin Heidelberg, 633 pp, ISBN 978-3-662-45200-4, ISBN 978-3-662-45201-1 (eBook). https://doi.org/10.1007/978-3-662-45201-1_1

Rasul NMA, Stewart ICF, Nawab ZA (2015) Introduction to the Red Sea: its origin, structure and environment. In: Rasul NMA, Stewart ICF (eds) The Red Sea: the formation, morphology, oceanography and environment of a young ocean basin. Springer Earth System Sciences, Berlin Heidelberg, pp 1–28. https://doi.org/10.1007/978-3-662-45201-1_1

Trommer G, Siccha M, Rohling EJ, Grant K, van der Meer MTJ, Schouten S, Baranowski U, Kucera M (2011) Sensitivity of Red Sea circulation to sea level and insolation forcing during the last interglacial. Clim Past 7:941–955. https://doi.org/10.5194/cp-7-941-2011

The Tides of the Red Sea

2

David T. Pugh, Yasser Abualnaja and Ewa Jarosz

Abstract

This paper describes the present tidal regime in the Red Sea. Both the diurnal and the semidiurnal tidal amplitudes are small because of the constricted connection to the Gulf of Aden and the Indian Ocean, at the Bab el Mandeb Strait. Semidiurnal tides have a classic half-wave pattern, with a central amphidrome, zero tidal range, between Jeddah and Port Sudan. We present a high resolution numerical model output of several tidal constituents, and also model the amphidrome position in terms of ingoing and outgoing tidal Kelvin waves. We quantify the energy budgets for fluxes and dissipation.

Introduction

The Red Sea is a semi-enclosed, narrow basin that extends between latitudes 12.5°N and 30°N, with an average width of 220 km, a mean depth of 524 m (Morcos 1970; Patzert 1974), and maximum recorded depths of about 3000 m. Toward the north, it ends in two narrow gulfs, the Gulf of Suez with an average depth of 40 m and the Gulf of Aqaba with depths over 1800 m (Fig. 2.1a, b). The only significant opening to the Indian Ocean is at its southern end through the shallow and narrow Bab el Mandeb Strait (a sill depth of 160 m and a minimum width of about 25 km) where it communicates with the Gulf of Aden.

D. T. Pugh (✉)
National Oceanography Centre, Joseph Proudman Building, 6 Brownlow Street, Liverpool, L3 5DA, UK
e-mail: d.pugh@me.com

Y. Abualnaja
Red Sea Science and Engineering Research Center, King Abdullah University of Science and Technology (KAUST), Thuwal, Saudi Arabia

E. Jarosz
Naval Research Laboratory, Oceanography Division Stennis Space Center, Stennis Space Center, MS 39529, USA

Seas that are connected with the open ocean through narrow straits are generally characterized by small tidal ranges (Defant 1961). Because of the restricting Bab el Mandeb Strait, the Red Sea tides are relatively small compared with those of the open ocean, and with those generally experienced along coasts near continental shelves. The semidiurnal oscillations predominate with maximum ranges on spring tides of about one metre in the far north at Suez, and in the southern entrance near Perim Island.

The length and depth of the Red Sea give near-resonant half-wavelength dynamics for the semidiurnal tide, which on a rotating Earth results in a wave progression around an amphidrome (a point with zero tidal amplitude) roughly located between Jeddah and Port Sudan, as shown in Fig. 2.2. The diurnal tides are only a few centimetres in range throughout the Red Sea, being most evident in the records from around Port Sudan, in comparison with the locally very small semidiurnal tidal ranges.

In the north, where the Red Sea divides into the Gulf of Aqaba and the Gulf of Suez, the two marginal gulfs have very different tidal regimes. The Gulf of Suez is shallow and interspersed with small islands. It has a mean depth of 36 m, and a natural period of 6.7 h; there is a semidiurnal amphidrome in the Gulf of Suez, and the strong currents imply an area of high local tidal energy dissipation.

The Gulf of Aqaba has a mean depth of 650 m and a natural oscillation period of about 0.9 h (Defant 1961). The Gulf of Aqaba tides oscillate in phase with the adjacent Red Sea with a 35 min lag from the entrance at the Strait of Tiran, to the head of the Gulf, typical of a standing wave (Monismith and Genin 2004). Tidal currents in the Gulf of Aqaba appear to be associated with internal wave generation; as tidal currents flow through the Strait of Tiran, they drive internal tidal waves on the internal density interface. Their strength varies considerably throughout the year, influenced by varying density stratification.

Despite the small tidal range, the semidiurnal tide of the Red Sea has been important in the development of general scientific ideas about the tides, as discussed by Defant

N. M. A. Rasul and I. C. F. Stewart (eds.), *Oceanographic and Biological Aspects of the Red Sea*, Springer Oceanography, https://doi.org/10.1007/978-3-319-99417-8_2

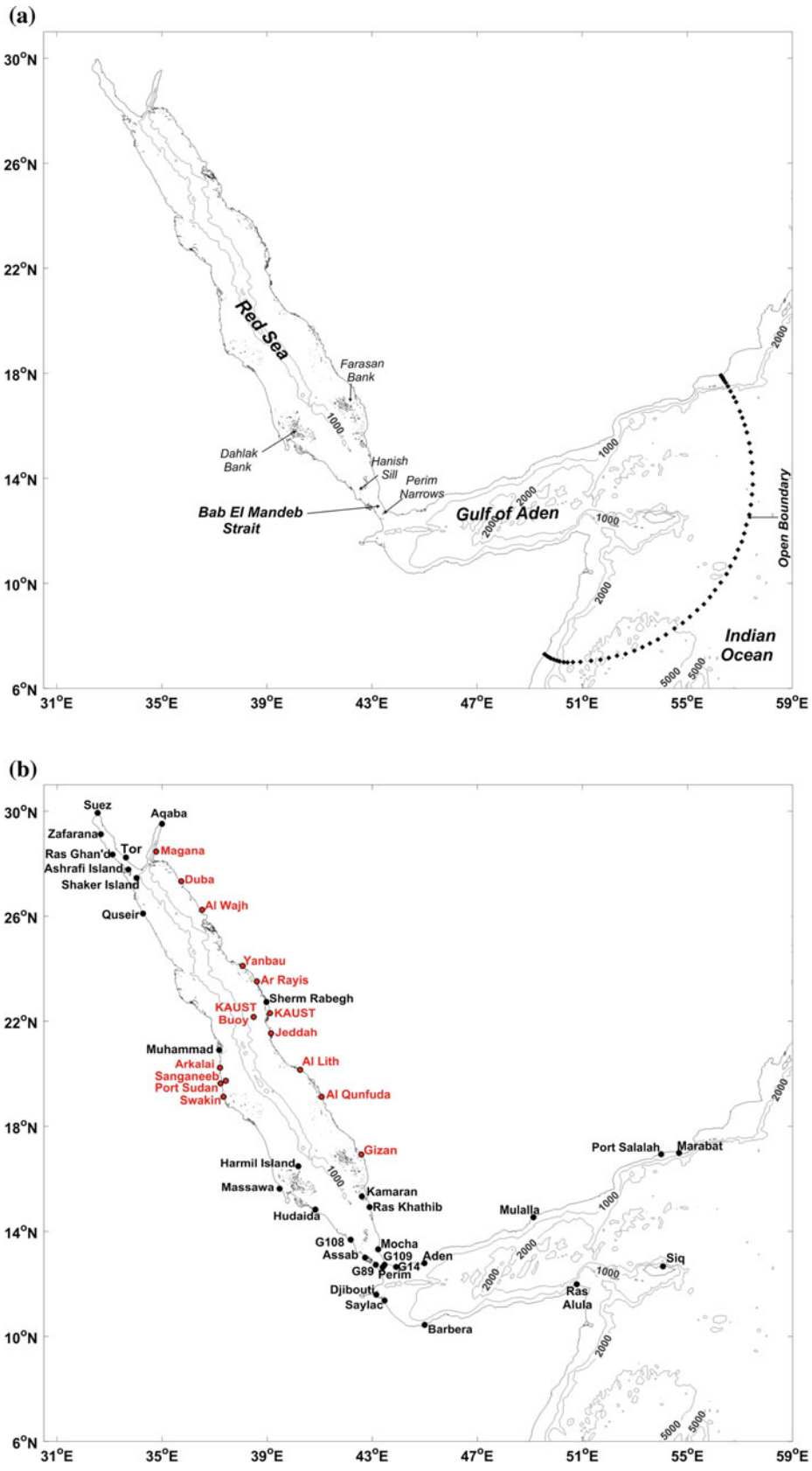

Fig. 2.1 **a** Map of the Red Sea, Bab el Mandeb Strait, Gulf of Aden and northwestern Indian Ocean, Dahlak and Farasan Banks, and the open ocean boundary of the model (dotted line); depth contours are in metres; **b** Locations of the sea level stations from heritage data subsurface pressure gauges (G89, G108, G109) all black circles. Those marked in red are sites of new observations for this study

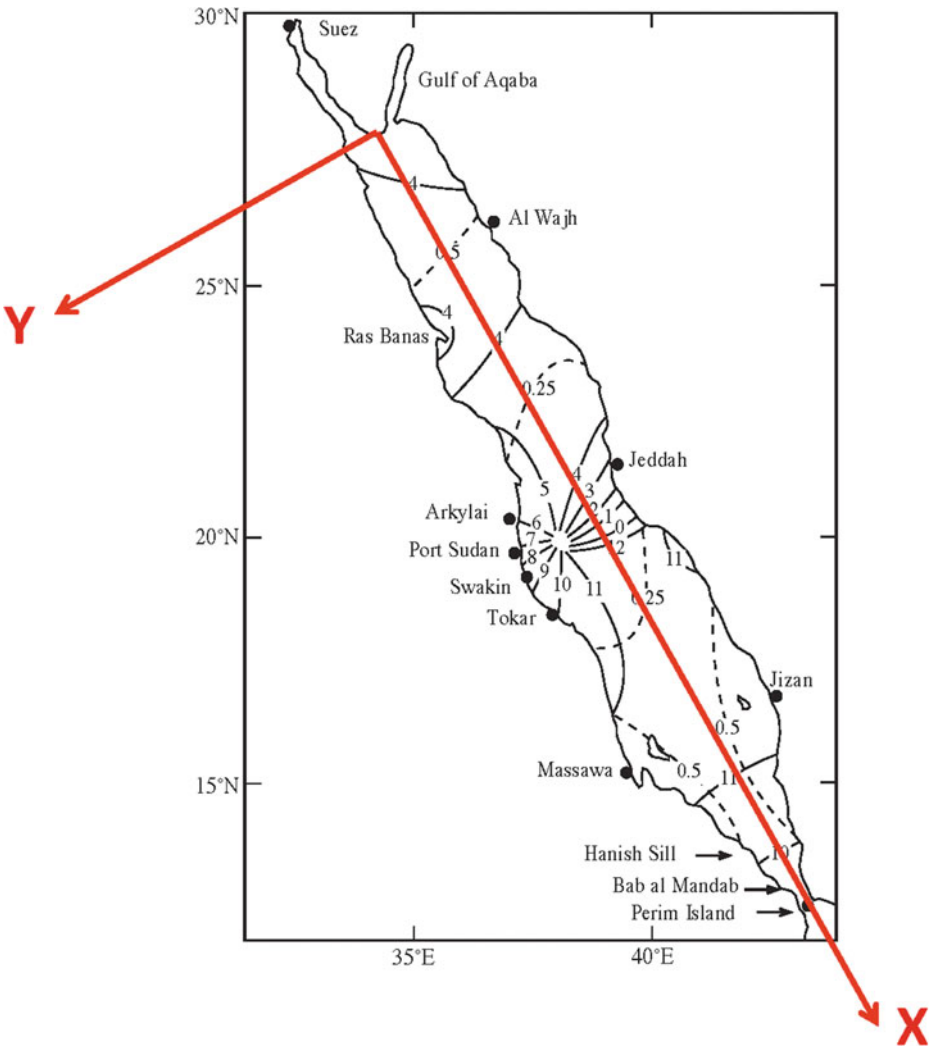

Fig. 2.2 Outline map of the semidiurnal lunar tidal range ($\mathbf{M_2}$) in the Red Sea and locations of the recent measurements. The coordinate X–Y system is used for fitting Kelvin waves in Sect. 6 (DHI 1963)

(1961). Harris (1898) was the first to explain dynamically the tides in the Red Sea in terms of the superposition of a standing wave produced by the tide generating forces and a progressive wave entering through the Bab el Mandeb Strait. Because of its long narrow shape and deep sides, the Red Sea was used as an early application of numerical computations of tides, before modern computer power made tidal modelling routine (Grace 1930). Proudman (1953) by modeling the Red Sea as 39 transverse sections along the axis, derived the behaviour of Red Sea tides as seiches in a one-dimensional basin; he also studied the influence of direct gravitational forcing within the Sea, in both cases without Earth rotation. The relative importance of tidal forcing through the Bab el Mandeb Strait, compared with direct gravitational forcing within the Red Sea itself, remained unclear. Defant (1961) called these external and direct forcing the *co-oscillating* and *independent* tides respectively; he suggested they are equally important, but also recommended consideration of the frictional energy losses, for a fuller description of the tidal dynamics.

Further recent evidence to help understand the Red Sea tidal budgets and energy dissipation, comes from detailed surveys of levels and currents at the southern end of the Red Sea (Jarosz et al. 2005a, b; Jarosz and Blain 2010). These surveys show a complicated system of tides with an amphidrome for $\mathbf{M_2}$ between the Perim narrows and the Hanish Sill. Tides to the south, in the Perim Narrows are similar to those in the Gulf of Aden. Amplitudes become very small near Assab and then increase northward to the co-oscillating amplitudes shown in Fig. 2.2. The numerical model simulation developed for Jarosz and Blain (2010), which included the full Red Sea, is the one used here, but whereas in that paper the emphasis was on the details of the southern Perim Narrows tides, here we look at the results from the model for the more extensive Red Sea, and compare them with a series of new high quality Red Sea tidal analyses which were not available at that time.

The very high resolution model of the Red Sea tides, with both external and direct gravitational forcing, is described in detail. The results are then used to investigate the detailed

location and movement of the central semidiurnal amphidrome; we interpret these movements in terms of a model of a standing wave consisting of two Kelvin waves, one travelling northward along the Saudi Arabian coast, and a reflected wave travelling south along the Egyptian and Sudanese coast. We also address the traditional tidal question for the Red Sea: The relative importance of direct gravitational tidal forcing, and the external forcing by tides at the Bab el Mandeb Strait (Defant 1961). A general overview of sea level variability in the Red Sea, including weather, climate and tectonic effects, was published in an earlier volume in this series (Pugh and Abualnaja 2015).

Data Collection

Before discussing the details of the recent data collection programme, it is appropriate to outline the prior state of knowledge, and of sea level data availability. In short, apart from information published by Vercelli (1925, 1927, 1931) and by Defant (1961), and the secondary port data published in nautical tide tables, until recently there has been very little robust sea level data available for analysis. In many cases, much of the published values in these tide table volumes are based on only a few days of observational data. The longest periods of data were from Port Sudan. Scientific sea level research with these data includes (Sultan et al. 1995; Sultan and Elghribi 2003), Elfatih (2010), and Mohamad (2012) (see Pugh and Abualnaja (2015) for a full listing). Satellite altimetry data has provided an alternative perspective.

Coastal in Situ Data

These earlier coastal data were systematically collected and tabulated as a preparation for the numerical model of Red Sea tides which we detail later (Jarosz and Blain 2010). This numerical model was developed at the United States Naval Research Laboratory, as part of a joint KAUST-Woods Hole Oceanographic Institution physical oceanography research programme. The results have not previously been published in open scientific literature.

In Table 2.1, the tidal harmonic constituents actually in the Red Sea, collected for the Red Sea modelling project entitled "Observation and Modeling—an Integrated Study of the Transport through the Strait of Bab el Mandab" (the BAM project) (see also Murray and Johns 1997) are listed. These consist of data at 22 water level stations, including three subsurface pressure gauges. The three subsurface pressure gauges were deployed for the BAM study. The model also uses data from other sites outside the Red Sea. Data and geographical locations of the water level stations were obtained from the listings of the International Hydrographic Organization (1979). It must be noted that all the observed tidal amplitudes and phases come from near-coastal areas, so there is no check directly of the tidal elevations in open waters, and that many values are based on only short periods of data. In addition, as explained above, at some water level stations only a few tidal constituents were available for the comparison; the common constituents for all stations were $\mathbf{O_1}$, $\mathbf{K_1}$, $\mathbf{M_2}$, and $\mathbf{S_2}$. These are the principal lunar diurnal term $\mathbf{O_1}$, the luni-solar diurnal term $\mathbf{K_1}$, the principal semidiurnal lunar tide $\mathbf{M_2}$ and the principal semidiurnal solar tide $\mathbf{S_2}$. The locations are plotted in Fig. 2.1b.

The model was also compared with tidal information for seven sites outside the Red Sea, in the Gulf of Aden, but inside the model boundary shown in Fig. 2.1. The full set of tidal data used for model comparison, together with fuller details of the process and maps of four additional modelled smaller tidal terms ($\mathbf{Q_1}$, $\mathbf{P_1}$, $\mathbf{N_2}$ and $\mathbf{K_2}$) is available in the original technical report (Jarosz and Blain 2010).

For the subsurface pressure measurements, G89, G108 and G109, additional caution is necessary when considering the $\mathbf{S_2}$ tidal constituent term. This is because subsurface pressures include changes in atmospheric pressures; it is appropriate to give some background information here.

In addition to gravitational forcing, there is another type of tidal forcing related to the solar heating variations, generally called *radiational forcing*. Detailed harmonic tidal analyses of atmospheric pressures show a daily constituent of 24 h period $\mathbf{S_1}$. In addition, there is an $\mathbf{S_2}$ constituent. Generally, the $\mathbf{S_1}$ constituent, representing diurnal air pressure changes, is a global tropical phenomenon, sometimes enhanced by the local diurnal land/sea winds; the radiational $\mathbf{S_2}$ constituent is driven by the twelve-hour oscillation of air pressure in the tropics. These air pressure tidal variations are included in subsurface pressure measurements, and must be corrected for. They are also, of course, potentially drivers of the measured marine tides.

Figure 2.3 shows the variations of air pressure over 5 days at KAUST, with both diurnal and semidiurnal components.

By the usual inverted barometer arguments, the atmospheric $\mathbf{S_2}$ low atmospheric pressures which occur globally at approximately 04:00 and 16:00 local time, are equivalent to a maximum sea level increase of 12.5 mm at the equator. In the Red Sea, the $\mathbf{S_2}$ atmospheric tide has an amplitude in the range 0.9–1.1 mbar (9–11 mm), decreasing with increasing latitude. The phase increases from east to west from 210 to 240 degrees relative to Greenwich, giving maximum pressures between 10:00 and 11:00 local time, and another pressure maximum between 22:00 and 23:00 local time (Ray and Ponte 2003).

However, the problem in making this correction in a specific region is that we cannot know the extent of the local

Table 2.1 Summary of earlier Red Sea tidal information, used for calibrating the numerical model. Amplitudes (H) in centimetres, phases (G) in UT. The final two columns show the amplitude ratio for the two principal semidiurnal tides, 0.46 in the Equilibrium Tide forcing; and the phase differences which are also the *age of the tide,* the number of hours after new and full moon that the maximum (spring) tides occur. Consistency of these parameters within sets of analyses is an indication of robust processes

	Location	Latitude (N)	Longitude (E)	O1		K1		M2		S2		H (S2/M2)	G (S2-M2)
				H	G	H	G	H	G	H	G		
1	Perim	12.63	43.40	18.0	351	35.0	350	37.0	136	17.0	159		
2	G89	12.73	43.13	15.0	345	30.0	340	23.0	121	14.0	142	0.61	21
3	G109	12.73	43.47	15.0	345	30.0	340	29.0	125	16.0	144	0.55	19
4	Assab	13.00	42.73	8.5	344	18.0	335	6.9	259	4.0	170	0.58	−89
5	Mocha	13.32	43.23	6.1	352	7.0	335	8.0	244	4.5	188	0.56	−56
6	G108	13.68	42.18	2.0	335	6.0	321	24.0	286	5.0	299	0.21	13
7	Hudaida	14.83	40.83	1.0	92	1.0	340	30.0	305	6.0	351	0.20	46
8	Ras Khathib	14.92	42.90	1.0	82	4.0	69	26.0	294	7.0	332	0.27	38
9	Kamaran	15.33	42.60	1.0	140	2.0	34	33.0	300	9.0	334	0.27	34
10	Massawa	15.62	39.47	2.0	184	2.3	16	33.4	328	12.4	332	0.37	4
11	Harmil Island	16.48	40.18	1.0	180	2.0	166	13.0	318	3.0	334	0.23	16
12	Port Sudan	19.60	37.23	2.0	170	2.0	168	1.0	204	1.0	256	1.00	52
13	Muhammad	20.90	37.17	2.0	175	3.0	166	6.0	132	1.0	185	0.17	53
14	Jeddah	21.52	39.13	1.0	161	2.8	156	6.0	109	1.0	132	0.17	23
15	Rabegh	22.73	38.97	4.0	162	4.0	156	11.0	124	2.0	165	0.18	41
16	Quseir	26.10	34.27	2.0	192	2.0	158	22.0	112	5.0	139	0.23	27
17	Shaker Island	27.45	24.03	1.0	178	2.0	167	25.0	117	4.0	144	0.16	27
18	Ashrafi Islands	27.78	33.72	1.0	153	2.0	167	25.0	118	4.0	145	0.16	27
19	Tor	28.23	33.62	2.0	159	4.0	164	8.0	205	1.0	230	0.13	25
20	Ras Ghan'd	28.35	33.12	2.0	157	2.0	160	18.0	274	7.0	302	0.39	28
21	Zafarana	29.12	32.67	1.0	199	3.0	165	42.0	280	12.7	301	0.30	21
22	Aqaba	29.52	35.00	1.0	146	2.0	158	28.0	128	8.0	155	0.29	27
23	Suez	29.93	32.55	1.3	170	4.5	158	56.0	278	14.0	306	0.25	28
				4.0		7.4		22.2		6.9		0.33	19.3

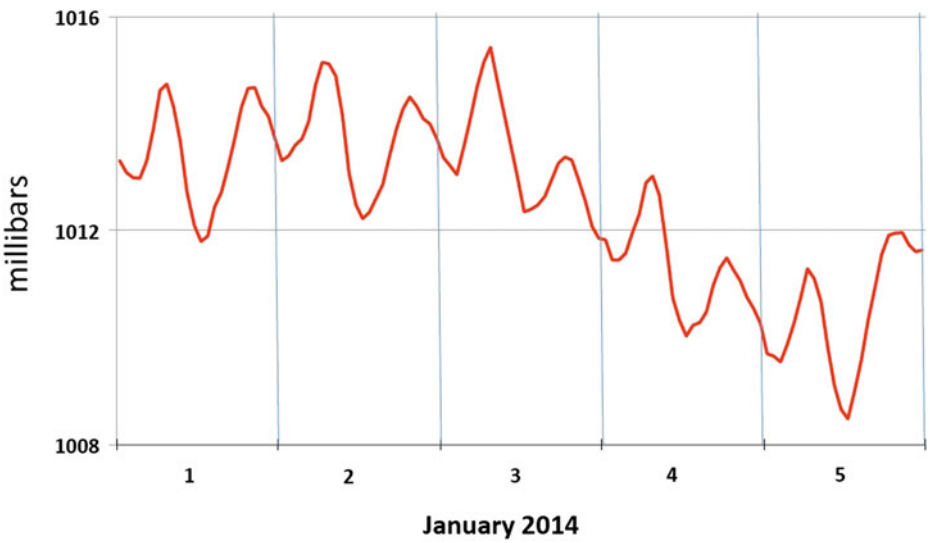

Fig. 2.3 Air pressures from the KAUST offshore buoy showing regular daily cycles

inverse barometer effect on sea levels. If the sea levels make a full and immediate inverted barometer response, then the subsurface pressures will be a measure of the gravitational tide. But if there is only partial compensation for the air pressure forcing the measured subsurface pressures will be both gravitational and partly radiational. For these reasons caution is necessary in analyses and hydrodynamic interpretation of the $\mathbf{S_2}$ tide and to a lesser extent the $\mathbf{K_1}$ tide, especially where the gravitational tides are small, for example near amphidromes.

To improve the availability of tidal constituents in the Red Sea, we have benefited from the recent long-period measurements, as given in Table 2.2. These fall into four groups:

- Subsea *pressure measurements* at four sites in Sudan, concentrated around the semidiurnal amphidrome; these were made with assistance from Elfatih Bakry Ahmed Eltaib, researcher in physical oceanography at the Institute of Marine Research, Red Sea University, Port Sudan;
- Three *subsurface pressure* measurements in Saudi Arabia, also near the amphidrome, as part of the KAUST Red Sea observing programme;
- Sea *level* data from seven sites, established since 2012 as part of the Saudi General Commission for Survey new sea level network. The seven General Commission for Survey permanent gauges along the whole length of the Saudi Arabia coast are high quality Aquatrak acoustic measurements of water levels;
- Current and air pressure measurements at the KAUST buoy mooring (Fig. 2.1b); the current components convention is: X positive along the Red Sea to the north, and Y positive across the Red Sea to the east.

The values of tidal amplitudes and phases for the major terms are summarised in Table 2.3. The final two columns in Table 2.3 show the ratio of the $\mathbf{S_2/M_2}$ amplitudes, and the $\mathbf{S_2}$ minus $\mathbf{M_2}$ phase differences in the tidal constituents. These values are a useful check on the consistency of the analyses among themselves, in the region. The one exception to the

Table 2.2 Locations of new sea level measurements and sources. Red Sea University IMR is located in Port Sudan; GCS is the Saudi General Commission for Survey. Gauge manufacturers are accessible on the Web

Location	Latitude (N)	Longitude (E)	Gauge	Parameter	Measuring authority	Months	Period
Swakin	19.12	37.34	RBR 420-TG	SSP	Red Sea University IMR	7.5	25 Feb 2013 to 7 Sept 2013
Port Sudan	19.63	37.22	RBR 420-TG	SSP	Red Sea University IMR	7.5	25 Feb 2013 to 7 Sept 2013
Sanganeeb	19.73	37.43	RBR 420-TG	SSP	Red Sea University IMR	6	14 May 2015 to 18 Oct 2015
Arkalai	20.23	37.20	RBR 420-TG	SSP	Red Sea University IMR	7.5	25 Feb 2013 to 7 Sept 2013
Al Lith	20.15	40.26	SBE Seagauge	SSP	KAUST	12	26 June 2013 to 15 June 2014
KAUST	22.31	39.11	RBR 420-TG	SSP	KAUST	6	6 Mar 2013 to 7 Sept 2013
Ar Rayis	23.52	38.61	SBE Seagauge	SSP	KAUST	12	5 June 2014 to 28 May 2015
Gizan	16.93	42.58	Aquatrak 5000	Level	GCS	12	1 April 2014 to 31 March 2015
Al Qunfuda	19.12	41.07	Aquatrak 5000	Level	GCS	12	1 April 2014 to 31 March 2015
Jeddah	21.54	39.15	Aquatrak 5000	Level	GCS	12	1 April 2014 to 31 March 2015
Yanbau	24.11	38.07	Aquatrak 5000	Level	GCS	12	1 April 2014 to 31 March 2015
Al Wajh	26.24	36.52	Aquatrak 5000	Level	GCS	12	1 April 2014 to 31 March 2015
Duba	27.33	35.73	Aquatrak 5000	Level	GCS	12	1 April 2014 to 31 March 2015
Magana	28.46	34.77	Aquatrak 5000	Level	GCS	12	1 April 2014 to 31 March 2015

Table 2.3 Principal tidal constituents from the new measurements listed in Table 2.2. See Table 2.1 for details of the final two columns. Note the increased consistency among the analyses for this new data. Data from the KAUST buoy are for air pressures and current measurements (see text)

Location	Latitude (N)	Longitude (E)		O1		K1		M2		S2		H(S2/M2)	G(S2-M2)
				H	G	H	G	H	G	H	G		
Swakin	19.12	37.34		2.1	159	3.4	168	1.0	176	1.3	245	1.30	69
Port Sudan	19.63	37.22		2.0	159	3.2	166	1.7	142	1.3	230	0.76	88
Sanganeeb	19.73	37.43		1.6	144	2.5	163	1.7	140	1.3	230	0.76	91
Arkalai	20.23	37.20		1.8	160	3.1	170	2.7	131	1.3	214	0.48	83
Al Lith	20.15	40.26		1.8	159	2.8	159	2.5	329	0.9	277	0.36	−52
KAUST	22.31	39.11		1.6	166	2.8	222	11.0	115	3.2	158	0.29	43
Ar Rayis	23.52	38.61		1.5	169	2.8	164	14.6	115	4.5	153	0.31	38
Gizan	16.93	42.58		1.7	136	2.1	132	32.0	295	10.4	326	0.33	31
Al Qunfuda	19.12	41.07		1.7	131	2.6	148	8.3	294	3.2	326	0.39	32
Jeddah	21.54	39.15		1.7	154	3.4	155	7.1	97	1.6	122	0.23	25
Yanbau	24.11	38.07		1.4	158	2.8	156	16.4	101	4.5	124	0.27	23
Al Wajh	26.24	36.52		1.1	159	3.4	146	23.3	103	6.9	124	0.30	21
Duba	27.33	35.73		1.1	161	2.6	157	24.9	103	7.1	125	0.29	22
Magana	28.46	34.77		1.0	169	2.4	152	27.5	110	8.0	135	0.29	25
KAUST Buoy	22.30	38.09											
		Air pressure (mb)	0.05	91	0.47	61	0.07	21	1.05	194			
		X currents (cm/s)	0.49	213	0.62	340	0.79	31	0.32	96			
		Y currents (cm/s)	0.67	135	0.88	217	1.87	59	0.92	52			
		deg/hour	**speed**		**13.94**		**15.04**		**28.98**		**30**		

general internally consistent pattern, is the phase difference et al. Lith, which is minus 52^0. Elsewhere the differences are always positive and locally consistent. This difference is a measure of the *age of the tide*, the time between new or full moon and maximum semidiurnal spring tidal ranges (see Pugh and Woodworth 2014, p. 76). For all the sea level measurements made by the Saudi General Commission for Survey, the age of the tide is from 21 to 32 h; for the sub-surface pressure measurements around Port Sudan the age is consistently around 70–90 h. This is probably due to the effects of the separate $\mathbf{M_2}$ and $\mathbf{S_2}$ amphidromes differing slightly as the $\mathbf{M_2}$ tidal wavelength is slightly longer (lower frequency). Similarly, the negative age et al. Lith can occur near an amphidrome. Also, the ages of the tides as measured on the pressure instruments may be affected by the air pressure and because of inexact adjustments for the $\mathbf{S_2}$ inverted barometer response discussed above.

For tides near the central semidiurnal amphidrome where the tidal signal is small and comparable with meteorological "noise", it is reasonable to ask whether repeated analyses can produce stable tidal constituents. Table 2.4 shows the results for four long-term KAUST measurements et al. Lith. The periods analysed are either a year, or in the first case six-months. For example, $\mathbf{M_2}$ has amplitudes which range between 2.4 and 2.5 cm, with phases between 327^0 and 331^0, a span equivalent to only eight minutes. This agreement from year to year is remarkably good even down to the one-millimetre level, and even applies to some very small gravitational terms such as the thrice-daily $\mathbf{M_3}$ term. This clearly shows that the actual observed tides are very stable at a fixed location even very close to the amphidrome.

Altimetry Data

The various long-term satellite altimetry missions have allowed tidal mapping from space using altimeter measurements of sea levels, generally with an accuracy of about 0.02 m. The sampling intervals, both in time and space call for very different analysis techniques from the traditional processing of regular measurements at fixed coastal sites. Figure 2.4 shows the co-tidal chart for the $\mathbf{M_2}$ tidal constituent for the Red Sea based on Topex/Poseidon measurements and inverse dynamic modelling techniques developed by Egbert and Erofeeva (2002). By solving in frequency space, otherwise considerable computational effort is much reduced. The web site for the Oregon State University offers tools for generating tidal maps for several

Table 2.4 Al Lith tidal constituents, showing the remarkable stability of the principal tidal constituents, from four different long periods of sub-surface pressure measurements, even at the millimetre level

Constituent	Speed			Amplitude (cm)						Phases (degrees)				
	Deg/h		2011	2012	2013–14	2014–15	Mean	Range	2011	2012	2013–14	2014–15	Mean	Range
O1	13.943		1.723	1.791	1.723	1.791	1.757	0.1	160	161	158	157	159	4
K1	15.0411		2.274	2.756	2.756	2.825	2.653	0.7	155	159	160	160	159	5
N2	28.4397		0.965	0.896	0.896	0.896	0.913	0.1	332	329	326	328	329	6
M2	28.9841		2.412	2.412	2.549	2.480	2.463	0.2	331	327	329	329	329	4
S2	30		0.896	0.896	0.965	0.896	0.913	0.1	278	277	276	277	277	3
K2	30.0821		0.276	0.345	0.276	0.276	0.293	0.1	317	326	320	320	321	9
M3	43.4761		0.345	0.276	0.276	0.207	0.276	0.1	283	282	301	312	295	29
Standard Dev (m) before analysis	0.15	0.18	0.20	0.20	**Data Blocks**	2011 May to November 2012								
Standard Dev (m) after analysis	0.08	0.09	0.10	0.11		2012 is November 2011 to December 2012								
Tidal variance %	33	25	24	27		2014 is June 2014 to May 2015								
Non-tidal variance %	67	75	76	73										

regions including the Red Sea, where the resolution is $1/60^0$. The Oregon State University package, called OTIS (OregonSU Tidal Inversion Software) captures ninety percent of the Red Sea sea-level variability in this map of the M_2 constituent (http://volkov.oce.orst.edu/tides/region.html). Agreement with the coastal observations is good, with all the general features reproduced. Local coastal differences from the general patterns, for example et al. Wajh, are not always captured.

Currents

The only available systematic measurements of currents are from the KAUST buoy system. The KAUST buoy is a long-term installation measuring currents with an acoustic current meter at several depths, air pressures, but not bottom pressures. The location is 22.30^0N, 38.09^0E, some 50 km off the Saudi coast, which at this latitude trends mainly south to north, rather than the overall Red Sea alignment of 23.5 degrees west of north. The water depth at the site is around 700 m.

The currents at the KAUST buoy were measured by an acoustic Doppler current meter, in 4 m depth levels. We averaged currents in the bands from 15 to 91 m depths, and resolved them into north and east components. Data were from 7 December 2014 to 28 February 2015. There was considerable vertical current shear and variability, but the averaged values as summarised in Table 2.5 were consistent. Note that the tidal currents are only about 10% of the observed current variance, or kinetic energy at this site.

Theoretical Background

Standing Waves

The two key factors in understanding the Red Sea tides are:

- Due to the length and depth of the Red Sea, a natural period of seiche is very close to that for half a semidiurnal tidal wavelength, and a quarter of a diurnal wavelength.
- The tidal amplitudes are small because of attenuation of external Indian Ocean forcing by the narrow Bab el Mandeb Strait in the south.

The resonant effect is explained as follows. For gravity oscillations of water in an enclosed basin the natural period is given by Merian's Formula:

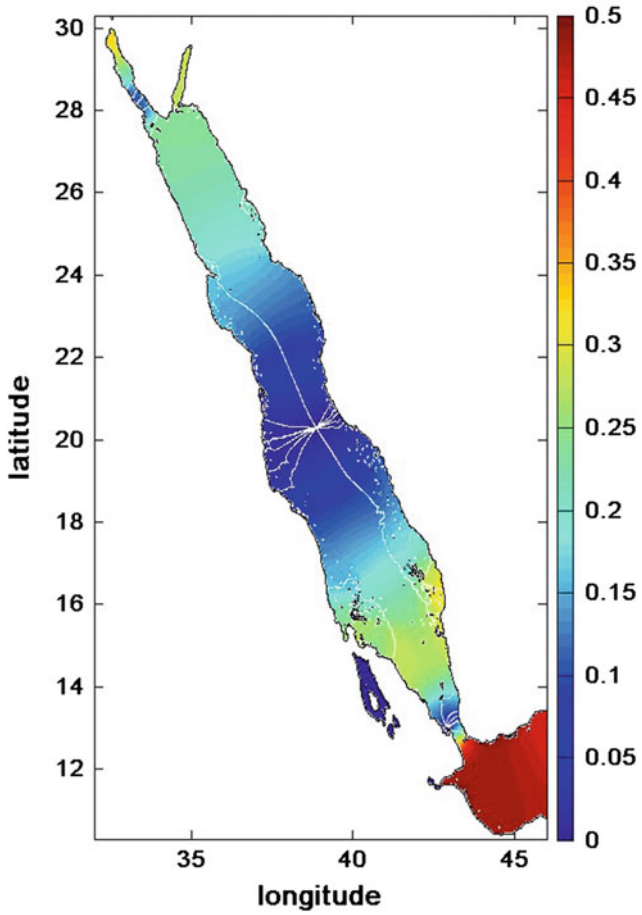

Fig. 2.4 Co-tidal $\mathbf{M_2}$ chart of the Red Sea based on altimetry data (Egbert and Erofeeva 2002). The lines running northwest and southeast along the Red Sea axis are 5 h and 11 h phase lag on UT, respectively

$$Natural\,period = \frac{2 \times sea\,length}{\sqrt{g \times water\,depth}} = \frac{2L}{\sqrt{gD}} \qquad (1)$$

For the Red Sea length of about 1600 km and a representative depth of 500 m the natural period is 12.6 h, close to semidiurnal resonance.

A Two-Wave Model

We can model the central Red Sea semidiurnal tide as two oppositely travelling Kelvin waves, because of the standing wave system. A brief theoretical description follows.

The forces that describe the motion of ocean currents in a rotating-Earth system cause a deflection of the currents toward the right of the direction of motion in the northern hemisphere and conversely in the southern hemisphere. The wave motion on this rotating system can be written as a Kelvin wave (Taylor 1920, 1922; Pugh and Woodworth 2014):

$$H(x,y,t) = H_0 \exp\left(\frac{-fy}{c}\right) \cos\left(\omega t - \frac{x}{c}\right) \qquad (2)$$

using a coordinate system as shown in Fig. 2.2. H is the water level, c is the wave speed $\sqrt{gD}$, and f is the Coriolis parameter. ω is the wave angular speed, t is the time variable and H_0 is the amplitude at $y = 0$.

Kelvin waves have the characteristic that rotation influences the way in which the wave amplitude decreases across the channel away from the value H_0 at the y = 0 boundary as shown in Fig. 2.5a (in the northern hemisphere). The wave heights and currents have amplitudes:

$$\begin{aligned} H(y) &= H_0 \exp\left(\frac{-fy}{c}\right) \\ U(y) &= \left(\frac{g}{D}\right)^{\frac{1}{2}} H(y) \end{aligned} \qquad (3)$$

Table 2.5 Comparison of observed and modelled currents at the KAUST buoy. Here X and Y directions are geographic east and north, not as in Fig. 2.2 and later amphidrome analyses

Observations												
		O1		K1		M2		S2	Tidal	Residual		Major axis	
	H	G	H	G	H	G	H	G	Variance	Current		Alignment	For M2
X (east)	0.49	213	0.66	340	0.79	31	0.32	96	20%	−12	cm/sec	17 degrees	East of north
Y (north)	0.67	135	0.88	217	1.88	59	0.92	52	8%	−8	cm/sec		
Model													
X (east)	0.005	299	0.01	290	0.06	239	0.03	265				3 degrees	East of north
Y (north)	0.15	67	0.33	66	1.34	36	0.57	64					

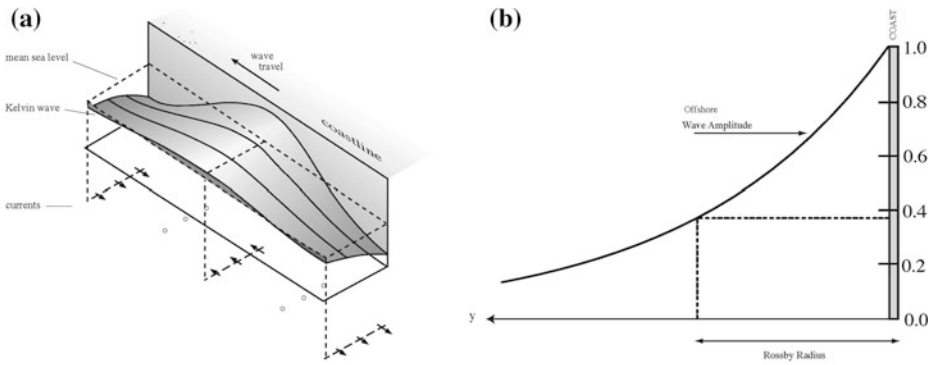

Fig. 2.5 K wave dynamics (after Pugh and Woodworth 2014): **a** A three-dimensional illustration of the elevations and currents for a Kelvin wave running parallel to a coast on its right-hand side (northern hemisphere). The normal dynamics of wave propagation are altered by the effects of the Earth's rotation which act at right angles to the direction of wave travel; **b** A two-dimensional section across the Kelvin wave at high tide, showing how the tidal amplitude falls away exponentially from the coast; at one Rossby radius the amplitude falls to 0.37 of the coastal amplitude. The wave is travelling into the paper

The exponential amplitude decay law has a scale length of c/f, which is called the barotropic Rossby radius of deformation. At a distance $y = c/f$ from y = 0 the amplitude has fallen to 0.37 H_0. The wave speed is the same as for a non-rotating case, and the currents are always parallel to the direction of wave propagation. Figure 2.5b shows the profile across a Kelvin wave. Note that Kelvin waves can only move along a coast in one direction; this is with the coast on the right in the northern hemisphere.

Figure 2.6 shows the co-tidal (equal phase) and co-amplitude (equal amplitudes and ranges) lines for a Kelvin wave reflected without energy loss at the head of a rectangular channel (Taylor 1922). The sense of rotation of the wave around the amphidrome is anticlockwise in the northern hemisphere and clockwise in the southern hemisphere. The co-tidal lines all radiate outward from the amphidrome and the co-amplitude lines form a set of nearly concentric circles with the centre at the amphidrome at which the amplitude is zero. The amplitude is greatest around the boundary of the basin. Figure 2.7 shows this displacement increasing as the reflected Kelvin wave is made weaker (Pugh 1981).

For a reflected Kelvin wave, the first amphidrome, where the incident and reflected waves cancel, is located at a position:

$$x = \frac{\pi c}{2\omega} \tag{4a}$$

$$y = \frac{-c \ln \alpha}{2f} \tag{4b}$$

Here α is the amplitude ratio of the reflected wave to the incident wave. In the Red Sea, the semidiurnal tides are approximately a standing wave in an almost enclosed narrow basin on the rotating Earth. A standing tidal wave is represented by two Kelvin waves, travelling in opposite directions. The tidal progression rotates about the nodal point, which is a central tidal amphidrome.

The incoming wave travels northward with a maximum amplitude along the coast of Saudi Arabia. At the northern end, the shallow water of the Gulf of Suez is a locally important area of energy loss due to the strong tidal currents, and bottom friction. Because of the energy loss, the tidal wave is not perfectly reflected. The reflected southward, slightly weaker, wave has a maximum amplitude along the coast of Egypt, Sudan and Eritrea.

Because the reflected Kelvin wave is weaker than the incident Kelvin wave, the amphidrome is displaced from the centre of the channel to the left of the direction of the incident wave; hence the central semidiurnal amphidrome is displaced toward the Sudan coast.

In a narrow channel, an amphidromic point may move outside the left-hand boundary, and in this case, although the full amphidromic system shown in Fig. 2.6 is not present, the co-tidal lines will still focus on an inland point. This is called a virtual or degenerate amphidrome. The tides of the Gulf of Suez have this degenerate amphidrome characteristic.

The expressions in Eq. 4a for the amphidrome location in x and y have the advantage in separating the effects of the two physically variable quantities, the angular speed ω, and the amplitude attenuation coefficient of the reflected wave, α. The effects of each on the amphidromic position and movement are orthogonal to each other and so may be considered independently in the section below on locating the amphidrome.

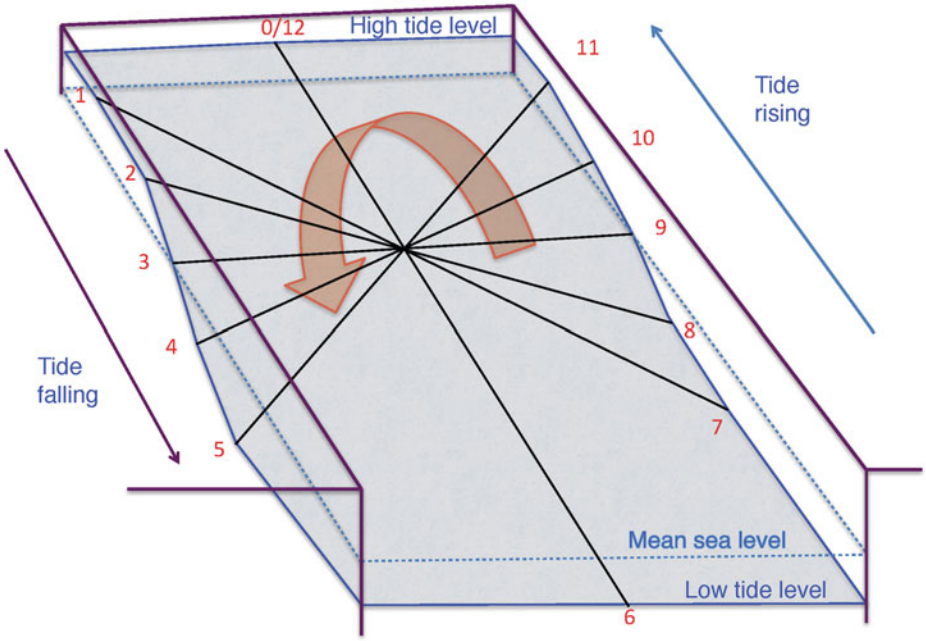

Fig. 2.6 Amphidrome dynamics: A three-dimensional drawing exaggerated to illustrate how a tidal wave progresses around an amphidrome in a basin in the Northern Hemisphere. The red numbers are hours in the semidiurnal cycle (after Pugh and Woodworth 2014)

Consider first the effect of changing angular speed ω on the x position. Although for a single tidal constituent the frequency and period are fixed, on a daily basis the frequency of the semidiurnal tides is slightly modulated, notably through a spring-neap 14 day cycle. This is because the speeds of $\mathbf{M_2}$ and $\mathbf{S_2}$, being 28.98^0/h and 30^0/h respectively, when combined have frequencies that vary in the range:

$$\frac{H_{M_2}\omega_{M_2} + H_{S_2}\omega_{S_2}}{H_{M_2} + H_{S_2}} \quad \text{and} \quad \frac{H_{M_2}\omega_{M_2} + H_{S_2}\omega_{S_2}}{H_{M_2} + H_{S_2}} \tag{5}$$

As we show in the section on locating the amphidrome, this range is from 29.29^0/h to 28.18^0/h for the Red Sea $\mathbf{M_2}$ and $\mathbf{S_2}$ amplitudes (Lamb 1932).

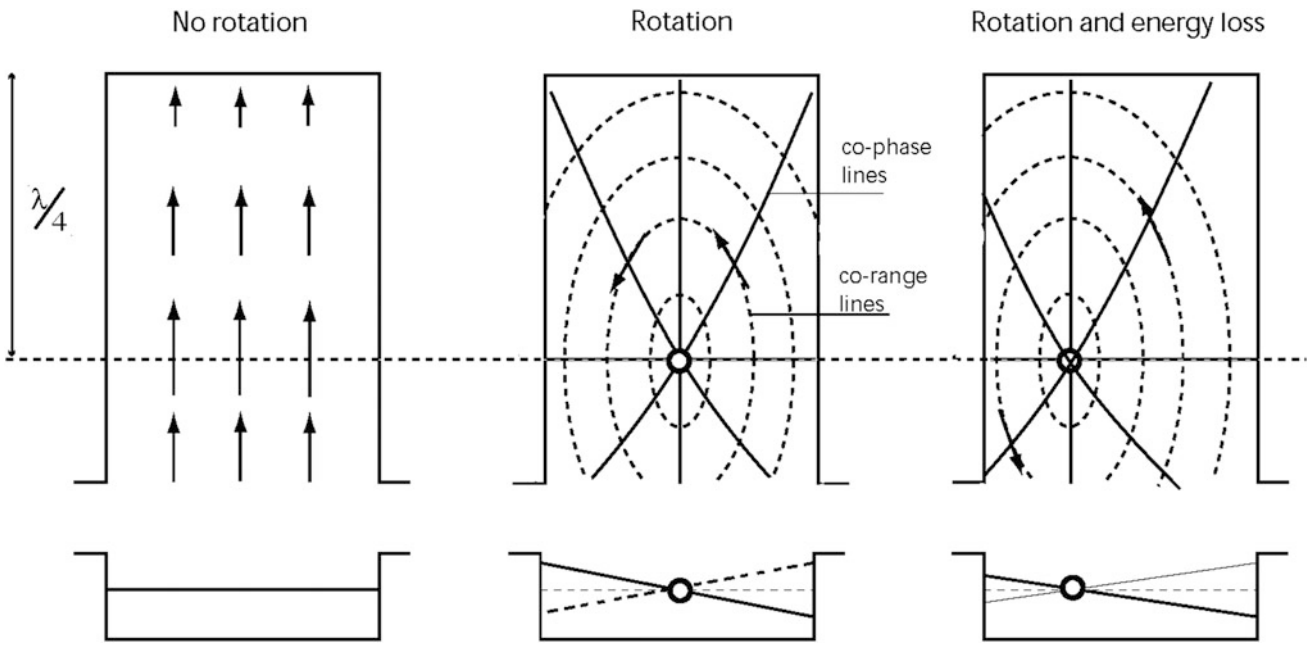

Fig. 2.7 Amphidrome dynamics: The effects of the Earth's rotation on a standing wave in a basin which is slightly longer than a quarter-wave length. With no rotation, there is a line of zero tidal amplitude. Because of the Earth's rotation, the tidal wave rotates around a point of zero amplitude, called an amphidromic point. In the third case, because the reflected wave has lost energy through tidal friction, the amphidrome is displaced from the centre line. (after Pugh and Woodworth (2014)

Numerical Modelling

Modelling Details

Yang et al. (2013) developed a two-dimensional finite element model of tides in the Red Sea and the Gulf of Aden. Their model boundary is in the Indian Ocean at 56^0E; at this boundary, the model is driven by predicted tides based on five constituents, $\mathbf{O_1}$, $\mathbf{P_1}$, $\mathbf{K_1}$, $\mathbf{M_2}$ and $\mathbf{S_2}$. There are 21836 triangular area sectors. The outputs from their model include co-tidal charts for the Gulf of Aden, and some small plots of $\mathbf{O_1}$, $\mathbf{K_1}$, $\mathbf{M_2}$ and $\mathbf{S_2}$ tides in the Red Sea, but there is little detail available.

Abohadima and Rakha (2013) developed a depth-integrated finite element model for the Red Sea to predict the tidal currents and tidal water level variations. The open boundary for their model is located at the Bab el Mandeb Strait, and the driver is the predicted levels at the Strait. The model had an element size varying from 15 km to less than 1 km. The output is only in terms of time variations of tidal levels and no attempt is made to look at individual tidal constituents in the elevations. The maximum tidal currents at springs are mapped, and show speeds of up to 20 cm/s. There is no direct gravitational forcing.

Madah et al. (2015) present a numerical model study of the Red Sea tides, with external forcing in the Gulf of Aden, 63434 grid cells, and 5 km grid spacing. They also reproduce the general tidal features, but check these against only limited observational data.

The numerical model results presented in this chapter are from Jarosz and Blain (2010), where fuller details are available. The model domain, shown in Fig. 2.1a, includes the Red Sea, Bab el Mandeb Strait, Gulf of Aden and the northwestern part of the Indian Ocean. The model area was chosen primarily to reproduce tidal waves propagating from the Indian Ocean, which is a significant forcing of tidal motion in the Red Sea as discussed by Defant (1961); having a more remote external model boundary avoids having a boundary in the locality of the complicated Bab el Mandeb Strait tidal dynamics. Depth information for the model was obtained from two sources: The Naval Oceanographic Office Digital Bathymetric Data Base-Variable Resolution (DBDB-V) (NAVOCEANO 1997) and charts published by the Defense Mapping Agency in 2006.

The finite element grid used in these computations is displayed in Fig. 2.8. It consists of 84,717 nodes and 163,854 elements. Nodal spacing for this mesh varies throughout the modelled region and ranges between 0.2 and 56 km with the highest refinement present in the Bab el Mandeb Strait and the Red Sea where the minimum and maximum nodal spacings are 0.2 and 5.5 km, respectively. The coarsest resolution is located in deep waters of the Gulf of Aden and Indian Ocean.

The two-dimensional form of the model is based on vertically integrated equations of motion and continuity, which, in a spherical coordinate system, are defined as follows (Gill 1982):

$$\frac{\partial U}{\partial t}+\frac{U}{R\cos\varphi}\frac{\partial U}{\partial \lambda}+\frac{V}{R}\frac{\partial U}{\partial \varphi}-fV-\frac{UV\sin\varphi}{R\cos\varphi} =-\frac{g}{R\cos\varphi}\frac{\partial}{\partial \lambda}(\zeta-\alpha\eta)-\frac{\tau_{b\lambda}}{\rho_0 H} \tag{6a}$$

$$\frac{\partial V}{\partial t}+\frac{U}{R\cos\varphi}\frac{\partial V}{\partial \lambda}+\frac{V}{R}\frac{\partial V}{\partial \varphi}+fU+\frac{UV\sin\varphi}{R\cos\varphi} =-\frac{g}{R}\frac{\partial}{\partial \varphi}(\zeta-\alpha\eta)-\frac{\tau_{b\varphi}}{\rho_0 H} \tag{6b}$$

$$\frac{\partial \zeta}{\partial t}+\frac{1}{R\cos\varphi}\frac{\partial (UH)}{\partial \lambda}+\frac{1}{R\cos\varphi}\frac{\partial (VH\cos\varphi)}{\partial \varphi}=0 \tag{6c}$$

where t represents time, λ, φ denote degrees of longitude and latitude, R is Earth radius, ζ is the free surface elevation, U and V are the depth-averaged horizontal east-and north-directed velocities, respectively, $H = \zeta + h$ is the total water column depth, h is the bathymetric depth relative to the geoid, $f = 2\Omega\sin\varphi$ is the Coriolis parameter, Ω is the angular speed of the Earth, ρ_o is a reference density, g is the acceleration due to gravity, α is the Earth elasticity Love Number factor approximated as 0.69 for all tidal constituents as used by other investigators including Schwiderski (1980) and Hendershott (1981) (the slight frequency dependency (Wahr 1981) is not important here), η is the Newtonian Equilibrium tidal potential, and $\tau_{b\lambda}$, $\tau_{b\varphi}$ are the bottom stresses taken as:

$$\tau_{b\lambda}=\rho_0 C_d U\sqrt{U^2+V^2};\quad \tau_{b\varphi}=\rho_0 C_d V\sqrt{U^2+V^2} \tag{7}$$

where C_d denotes the bottom drag coefficient.

The Equilibrium tidal potential is expressed as (Reid 1990):

$$\eta(\lambda,\varphi,t)=\sum_{n,j} C_{jn} f_{jn}(t_0) L_j(\varphi)\cos\left[2\pi(t-t_0)/T_{jn}+j\lambda+\upsilon_{jn}(t_0)\right] \tag{8}$$

where t is time relative to t_o, which is the reference time, C_{jn} is a constant characterizing the amplitude of tidal constituent n of species j, f_{jn} is the time-dependent nodal factor, υ_{jn} is the time-dependent astronomical argument, j = 0, 1, 2 are the tidal species (j = 0 declinational; j = 1 diurnal, j = 2 semidiurnal), $L_o = 3\sin^2\varphi - 1$, $L_1 = \sin(2\varphi)$, $L_2 = \cos^2\varphi$,